Transilient Turbulence Theory. Part II: Turbulent Adjustment

ROLAND B. STULL AND TAKEHIKO HASEGAWA[1]

Boundary Layer Research Team, Department of Meteorology, University of Wisconsin, Madison, WI 53706

(Manuscript received 21 February 1984, in final form 3 September 1984)

ABSTRACT

Turbulent adjustment is a scheme where dynamic instabilities in the flow are eliminated by turbulence. It is a form of first-order turbulence closure that is applicable to numerical forecast models of the atmosphere. The responsive form of transilient turbulence theory (developed in the companion paper) is shown to be identical to turbulent adjustment for mixing between two points in the vertical. For mixing in a column of many contiguous grid points in a numerical model, turbulent adjustment only approximates the atmosphere's tendency to eliminate instabilities; whereas, transilient turbulence better describes typical atmospheric responses by allowing large-eddy mixing. The utility of turbulent adjustment is demonstrated with a case-study one-dimensional simulation of the Wangara Day 33–34 boundary layer, where nocturnal stable-layer characteristics develop in response to surface forcings. Turbulent adjustment, although inefficient in its ability to eliminate instabilities, is much simpler and quicker-executing than transilient mixing, and might be useful in fine-mesh boundary-layer, cloud, and small-mesoscale models having short timesteps.

1. Introduction

A first-order turbulence theory called the transilient theory is developed in the companion paper, where mixing across finite distances is explicitly modeled. One of the turbulence parameterization schemes suggested there is responsive in nature, allowing turbulent mixing to react to dynamic instabilities induced in the mean flow.

Another type of responsive turbulence closure method is the turbulent adjustment technique used by Klemp and Lilly (1978). Turbulent adjustment reduces dynamic instabilities in a manner similar to the way that convective adjustment (Manabe *et al.*, 1965) reduces static instabilities. In this paper turbulent adjustment and transilient mixing are shown to be intimately related, and turbulent adjustment is applied to forecasting the mean state in the atmospheric boundary layer. Turbulent adjustment is shown to be a type of responsive transilient mixing that applies only in the vertical direction.

Turbulent adjustment is inherently local in nature; that is, any one pass of this adjustment scheme through a numerical model attempts to eliminate dynamic instabilities between vertically-adjacent pairs of grid points. Such a local adjustment differs from the bulk Froude number schemes of Thompson (1973) or Manins (1982), where bulk mixed-layer characteristics are used instead.

Potential applications of responsive methods include situations where numerical model grid spacings fall within the range of atmospheric eddy sizes. This could be large mechanical eddies in a pollutant dispersion model, thermals in a boundary layer model, or perhaps meso-scale circulations in a synoptic weather forecast model.

After a review of turbulent adjustment in Section 2, it is compared to transilient theory in Sections 3, 5 and 7. A multiple-pass turbulence adjustment scheme is shown in Section 4 to approximate large-eddy mixing. Application of turbulent adjustment is demonstrated for a Wangara-data case study in Section 6.

2. Turbulent adjustment between two points

When local vector wind shears ($d\mathbf{U}/dz$) are strong enough to create turbulence against the opposing buoyancy forces $[(g/\theta)d\theta/dz]$ in a statically stable environment, the air is dynamically unstable. The gradient Richardson number Ri is a measure of this instability

$$Ri = \frac{(g/\theta)d\theta/dz}{(d\mathbf{U}/dz)^2}.$$

If temperature and wind differences over a finite distance are known instead of local gradients, then the bulk Richardson number R_B is often used as an approximate indicator of instability

$$R_B = \frac{(g/\theta)\Delta\theta\Delta z}{(\Delta U)^2 + (\Delta V)^2}, \tag{1}$$

where Δ is the vertical difference operator.

In a nonturbulent flow, turbulence forms when Ri

[1] Present affiliation: Himeji LNG Terminal, Osaka Gas Company, Mega-Chisaki, Shirahama, Himeji-City, Hyogo, Japan T672.

falls below a critical value R_c. Turbulence tends to mix air from different points in the flow, creating a mixture with reduced vertical shears and gradients. In this manner the flow Richardson number increases. As mixing proceeds, a state is reached where there is insufficient instability to maintain turbulence. The turbulence then ceases when a termination value of the Richardson number R_T is reached. This is the turbulent adjustment (TA) process.

Woods (1969) suggested that a vertical resolution of better than $\Delta z = 50$ m is required to be able to use the local onset and termination values of $R_c = 0.25$ and $R_T = 1.0$. Coarser resolution implies that there is uncertainty about the imbedded local values. Larger values for the "bulk" critical Richardson numbers are therefore used with R_B, recognizing the associated uncertainty about the domain and even existence of turbulence (see discussion in the companion paper and Cahir *et al.*, 1976; Mahrt, 1981).

If one assumes that the TA mixes all variables proportionally, then

$$\frac{\Delta \mathbf{U}'}{\Delta \mathbf{U}} = \frac{\Delta\theta'}{\Delta\theta} = \frac{\Delta q'}{\Delta q} = \frac{\Delta U'}{\Delta U} = \frac{\Delta V'}{\Delta V} = 1 - P_M, \quad (2)$$

where the primes denote the new value of the variables after mixing, nonprimed variables indicate their initial values before mixing, (U, V) are the (x, y) components of wind vector $\mathbf{U}$, q is specific humidity, and P_M is defined as the proportion of mixing. Here P_M is zero for no mixing and unity for total mixing of the two layers. Note that total mixing is not required because turbulence may cease when the Richardson number becomes greater than R_T, even though a finite wind shear remains.

It is important to recognize that equations like (2) describe just one part of the physics governing atmospheric flows—namely the mixing. Other forcings such as pressure gradients for momentum, or diabatic heating for potential temperature, must still be accounted for. Thus, a typical application of TA involves the forecast of atmospheric variables using the equations of motion sans the turbulence terms. The TA scheme is then applied between each timestep, or less often to reduce computational demands. This approach is used in Section 6.

After mixing, the new Richardson number is specified to be no less than the termination value:

$$R_T = \frac{g\Delta\theta'\Delta z}{\theta(\Delta \mathbf{U}')^2}. \quad (3)$$

With a little algebraic manipulation, (2) and (3) are combined to give

$$P_M = 1 - \frac{R_B}{R_T}. \quad (4)$$

Knowing P_M, one can use (2) to calculate $\Delta\theta'$, $\Delta q'$, $\Delta U'$ and $\Delta V'$. By restricting P_M to be $0 \leq P_M \leq 1$, one limits R_B to $0 \leq R_B \leq R_T$. If $R_B > R_T$, then the air is dynamically stable and there is no mixing. If $R_B < 0$, then the air is statically unstable; a convective adjustment scheme is applicable here.

If properties such as column-averaged momentum and heat are conserved during the mixing process, then thicker layers will change less during mixing than thinner layers (see Fig. 1). Using θ as an example, one finds that the new values of θ in each layer are:

$$\left.\begin{aligned} \theta'_1 &= \theta_1 + \beta(\Delta\theta - \Delta\theta') \\ \theta'_2 &= \theta_2 + (\beta - 1)(\Delta\theta - \Delta\theta') \end{aligned}\right\},$$

where subscripts 1 and 2 refer to the respective grid points sketched in Fig. 1, and where the relative mass factor β is

$$\beta = \frac{\Delta P_2}{\Delta P_2 + \Delta P_1} \approx \frac{\Delta z_2}{\Delta z_2 + \Delta z_1},$$

where P is pressure. The last approximation is possible if the average densities at the two points are nearly equal. When the layers are equal in thickness, $\beta = 0.5$.

Using the preceding equations and knowing that $(\Delta\theta - \Delta\theta') = P_M\Delta\theta$ from (2), one concludes that

$$\left.\begin{aligned} \theta'_1 &= \theta_1 + \beta P_M \Delta\theta \\ \theta'_2 &= \theta_2 + (\beta - 1)P_M\Delta\theta \end{aligned}\right\}. \quad (5)$$

Similar equations can be written for U'_1, U'_2, V'_1, V'_2, q'_1, and q'_2. Thus (4) and (5) provide a simple way to adjust the primary variables of two grid points toward their dynamically stable values.

3. Comparison of turbulent adjustment to transilient theory

For simplicity consider the special case of two equal-thickness grid layers in a numerical model.

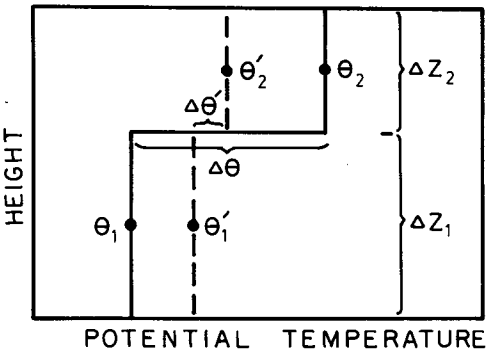

FIG. 1. Schematic of heat conservation when two layers of unequal thickness are turbulently adjusted. Potential temperature (θ) symbols with and without the prime denote post and premixing values, respectively. Each grid point is assumed to represent a layer average. Solid lines indicate the initial state, and dashed lines indicate the final state of the layers.

Transilient theory, allows us to model turbulent mixing for this case as

$$\left.\begin{aligned}\theta'_1 &= c_{11}\theta_1 + c_{12}\theta_2\\ \theta'_2 &= c_{21}\theta_1 + c_{22}\theta_2\end{aligned}\right\}, \tag{6}$$

using discrete transilient mixing coefficients c_{ij}. The conservation constraints discussed in the companion paper yield $c_{11} = c_{22}$ and $c_{12} = c_{21}$. Thus, the exchange hypothesis is automatically satisfied for this two-grid-point case.

With some manipulation, (6) can be rearranged to give

$$\frac{\Delta\theta'}{\Delta\theta} = c_{11} - c_{12}, \tag{7}$$

where $\Delta\theta = \theta_2 - \theta_1$. However, (2) gives this same ratio as $1 - P_M$. Thus

$$c_{11} - c_{12} \equiv 1 - P_M \equiv \frac{R_B}{R_T}. \tag{8}$$

For no mixing ($P_M = 0$) we find that $c_{11} = c_{22} = 1$ and $c_{12} = c_{21} = 0$, as expected. For complete mixing ($P_M = 1$) we find that $c_{11} = c_{12} = c_{21} = c_{22} = 0.5$, again expected.

More significantly, (8) provides a way to vary the transilient coefficients in response to mean flow dynamic instabilities (R_B/R_T) in a statically stable environment.

Reasonable coefficient values are also found from (8) for statically unstable conditions. If we apply (8) to a statically-unstable case where $R_B/R_T = -0.5$, then the resulting coefficients become $c_{11} = c_{22} = 0.25$ and $c_{12} = c_{21} = 0.75$. At greater instability, $R_B/R_T = -1.0$, the coefficients become $c_{11} = c_{22} = 0$ and $c_{12} = c_{21} = 1$. Both of these yield convective overturning, as would be expected. This is described in more detail in Section 5c. For static instabilities where $R_B/R_T < -1.0$, (8) cannot be used because it violates the entropy constraint discussed in Section 5d. For this free convection limit, it is better to invoke free-convection similarity arguments to scale the transilient coefficients, as is discussed in the companion paper.

Although transilient mixing is a general concept that can be applied to all directions, its use here is focused on vertical mixing. This allows vertical mixing to be responsive to Richardson number variations, similar to the behavior of TA. Other flow instabilities might be useful for defining horizontal transilient mixing coefficients, as discussed later.

4. Extension to multiple grid points

Turbulent adjustment as described by (4) and (5) is applied to a pair of adjacent grid points. Such a process is local in nature—not much different than a sophisticated K-theory approach where K is a function of R_B. However, in a column of many grid points, the adjustment of one pair of points often "unadjusts" neighboring pairs of points. A solution to this dilemma is achieved by making multiple adjustment passes through the column (Klemp and Lilly, 1978).

A multiple-pass procedure is not local in nature. For example, air from grid-point 1 might be mixed into point 2 during the first pass. During the second pass, any air mixed from point 2 into point 3 is also carrying some of the air that originally was at 1. The net result is that multiple-pass adjustment involves mixing between many grid points that are separated in space. This is nothing more than transilient mixing.

Mathematical techniques from the companion paper are useful in describing such a process. A single-pass TA is conveniently represented by a tridiagonal, symmetric matrix of transilient coefficients $\mathbf{C}(1)$ when applied to equally-spaced grid points:

$$\mathbf{C}(1) = \begin{bmatrix} c_{11} & c_{12} & 0 & 0 & 0 & \cdot \\ c_{12} & c_{22} & c_{23} & 0 & 0 & \\ 0 & c_{23} & c_{33} & c_{34} & 0 & \\ 0 & 0 & c_{34} & c_{44} & c_{45} & \\ \cdot & & & \cdot & \cdot & \cdot \\ \cdot & & & & \cdot & \cdot \end{bmatrix}. \tag{9}$$

The symmetry (exchange hypothesis) requirement reflects the proportional mixing assumption of (2).

The number n in $\mathbf{C}(n)$ denotes the minimum number of TA passes necessary to generate mixing expressed by the transilient array. As shown in the companion paper, the ith row of the matrix indicates the mixing into the ith gridpoint of a column of air, while the jth column indicates that the air is being mixed from the jth gridpoint. Thus c_{34}, for example, represents the fraction of air coming from gridpoint 4 that is mixed into gridpoint 3.

For some soundings, it is impossible to find values for the matrix elements in (9) that allow (3) to be satisfied on one pass. An example of such a sounding is given in Appendix A. The point to be made here is that failure to eliminate dynamic instabilities in one pass is not necessarily the fault of poor numerical algorithms. The failure lies in the assumption that mixing is restricted to adjacent grid points.

If $\mathbf{C}(1a)$ and $\mathbf{C}(1b)$ represent tridiagonal transilient matricies corresponding to the first and second single passes, respectively, then the overall mixing for two passes is $[\mathbf{C}(1a)][\mathbf{C}(1b)] \equiv [\mathbf{C}(2)]$. Thus, the effects of a two-pass turbulent adjustment can be accomplished in one step by using a transilient array of

$$\mathbf{C}(2) = \begin{bmatrix} c_{11} & c_{12} & c_{13} & 0 & 0 & 0 & 0 \\ c_{21} & c_{22} & c_{23} & c_{24} & 0 & 0 & 0 \\ c_{31} & c_{32} & c_{33} & c_{34} & c_{35} & 0 & 0 \\ 0 & c_{42} & c_{43} & c_{44} & c_{45} & c_{46} & 0 \\ 0 & 0 & c_{53} & c_{54} & c_{55} & c_{56} & c_{57} \\ & & & \cdot & \cdot & \cdot & \cdot \\ & & & & \cdot & \cdot & \cdot \end{bmatrix}.$$

Even the equivalent of two passes may be insufficient to eliminate all dynamic instabilities. The extension to multiple-pass adjustment is straightforward in concept, and is thus not written here.

Although a spectrum of eddy sizes involves mixing between many points separated in space, this mixing is not instantaneous (see the companion paper). Thus, in a numerical model taking sufficiently small timesteps, we should not necessarily require the total elimination of dynamic instabilities during any one timestep. For such cases, the one- or two-pass-per-timestep TA may adequately approximate the mixing tendency of turbulence, and is often more desirable than a full transilient mixing description because of the speed and simplicity of the TA algorithms. Klemp and Lilly (1978) chose the single pass approach as being adequate for their purposes.

In the remainder of this paper, TA and transilient mixing will be treated as two separate procedures for implementing the single process of turbulence response to dynamic instabilities.

5. Mixing, overturning and entropy

The following discussion elucidates some additional concepts and constraints that aid in transilient coefficient parameterization.

a. Mixing coefficients and Richardson numbers

Not only can we calculate R_B for each pair of adjacent grid points in a column, but we can calculate Richardson numbers between points that are further apart. For any column of n grid points we can form an array of Richardson numbers from each of the $n(n-1)/2$ independent combinations of the grid-point pairs:

$$\mathbf{R}_B = \begin{bmatrix} — & r_{12} & r_{13} & r_{14} & \cdots & r_{1n} \\ & — & r_{23} & r_{24} & \cdots & r_{2n} \\ & & — & r_{34} & \cdots & r_{3n} \\ & & & — & \cdots & \vdots \\ & & & & — & r_{(n-1)n} \\ & & & & & — \end{bmatrix} \tag{10}$$

where any element r_{ij} represents the bulk Richardson number between grid points i and j. The lower half of the matrix, not printed, is a reflection of the upper half because $r_{ij} = r_{ji}$, and r_{ii} is undefined.

By analogy with (8) we can try to construct a responsive transilient matrix for n grid points

$$\mathbf{c} = \begin{bmatrix} c_{11} & c_{12} & c_{13} & c_{14} & \cdots & c_{1n} \\ & c_{22} & c_{23} & c_{24} & \cdots & c_{2n} \\ & & c_{33} & c_{34} & \cdots & c_{3n} \\ & & & c_{44} & \cdots & \vdots \\ & & & & & c_{nn} \end{bmatrix} \tag{11}$$

using the known Richardson numbers from (10). The exchange hypothesis used to make (11) symmetric also means that state and mass conservation collapse into just one conservation law, such as the mass conservation used here:

$$\sum_{j=1}^{n} c_{ij} = 1$$

for each i (see the companion paper).

The $n(n-1)/2$ known forcings from (10) with the n known mass-conservation constraints give sufficient knowns from which to calculate the $n(n+1)/2$ unknown transilient elements of (11). A parameterization to construct the appropriate relationship between $\mathbf{R}_B$ and $\mathbf{c}$ was suggested in the companion paper.

b. Domains of turbulence

Out of a column of n grid points a subset of m might be dynamically unstable. A transilient array of size m is adequate for handling the mixing. For a prescribed *a priori* mixing approach, as was discussed in the companion paper, the transilient array must be limited to m to prevent mixing into nonturbulent regions. For a responsive approach, however, the full array of size n may be used with the values of the coefficients defining the domains of turbulence.

For example, a transilient array of

$$\begin{bmatrix} c_{11} & c_{12} & c_{13} & 0 & 0 & 0 \\ c_{21} & c_{22} & c_{23} & 0 & 0 & 0 \\ c_{31} & c_{32} & c_{33} & 0 & 0 & 0 \\ 0 & 0 & 0 & 1 & 0 & 0 \\ 0 & 0 & 0 & 0 & c_{55} & c_{56} \\ 0 & 0 & 0 & 0 & c_{65} & c_{66} \end{bmatrix}$$

allows two separate patches of turbulence. One patch between grid points 1–3, and the other between 5–6, with no mixing to or from grid point 4. Coefficients such as c_{15} and c_{62} must be zero. Otherwise turbulent exchange across a nonturbulent layer would be implied, which is clearly unrealistic.

Even if a Richardson number r_{15} for example, is below the critical value for turbulence, there may not be turbulence over that whole subdomain (grid points 1–5) if still smaller subdomains (such as grid point 4) are nonturbulent. Thus, for any Richardson number $r_{i,i+k}$, highest priority in determining the turbulent domain should be given to Richardson numbers with $k = 1$, such as r_{23}, r_{34} or r_{78}. In other words, a turbulent domain is defined by a contiguous subcolumn of grid-points, j to $j+m$, each of which satisfy $r_{i,i+1} < R_c$ for $i = j$ to $j+m-1$.

Probably densities of vertical turbulence velocities w, such as shown by Lenschow (1970), demonstrate the finite range of speeds typically observed. In any specified time interval t, air will be transported a distance wt. The observation that the probability

density decreases as transport distance increases implies that the rate of mixing between two points c_{ij} decreases as separation distance $|i - j|$ increases. Similar assumptions were made by Fiedler (1984).

Thus, $c_{i,i+k}$ should decrease as k increases, regardless of how far below critical the corresponding Richardson number $r_{i,i+k}$ is. It is usually appropriate to include such distance-weighting into those responsive methods that parameterize **c** as a function of **r**. Shorter timesteps are associated with shorter drop-off distances of the domain of influence of turbulence (see the companion paper).

c. *Convective overturning*

Negative Richardson numbers are usually associated with flow that is statically unstable as well as dynamically unstable. Convection, the flow response to static instabilities, involves the transport of warm air upward in thermals and cold air downward. Turbulent mixing usually prevents the total convective overturning situation where air from the top and bottom of a column simply trade places.

The range of convection from simple overturning to complete mixing is easily described with transilient coefficient arrays. For a two grid-point domain, simple overturning (total exchange), overturning with mixing (partial exchange), and complete mixing are exemplified by transilient coefficient arrays:

$$\begin{bmatrix} 0 & 1 \\ 1 & 0 \end{bmatrix}, \quad \begin{bmatrix} 0.25 & 0.75 \\ 0.75 & 0.25 \end{bmatrix}, \quad \begin{bmatrix} 0.5 & 0.5 \\ 0.5 & 0.5 \end{bmatrix}.$$

Another example of extreme overturning is where the two middle levels and the top and bottom levels are interchanged when multiplied by the following transilient matrix:

$$\begin{bmatrix} 0 & 0 & 0 & 1 \\ 0 & 0 & 1 & 0 \\ 0 & 1 & 0 & 0 \\ 1 & 0 & 0 & 0 \end{bmatrix}.$$

Care must be taken when numerically modeling total exchange, because the CFL numerical stability requirement must be satisfied (see Part I).

d. *Entropy*

If entropy and randomness increase in a mixing process, then negative transilient coefficients are not allowed.

If such were not the case, then turbulence would increase shears and strengthen lapse rates within the turbulent domain. As an example, the following transilient array satisfies conservation of mass and state and it even satisfies the exchange hypothesis; however, it violates the second law of thermodynamics by reducing randomness:

$$\begin{bmatrix} 1.10 & -0.10 \\ -0.10 & 1.10 \end{bmatrix}.$$

If this is applied to potential temperatures of $\begin{bmatrix} 310 \\ 300 \end{bmatrix}$ for example, then the temperature profile after transilient "mixing" is $\begin{bmatrix} 311 \\ 299 \end{bmatrix}$. Clearly, this is incorrect because mixing between two points should reduce discontinuities, not strengthen the differences.

Some organized atmospheric circulations can maintain sharp discontinuities or thermal microfronts against the mixing action of turbulence. One example is the boundary-layer thermal (Kaimal and Businger, 1970). Wind shear on a scale larger than the turbulent eddies can be one mechanism for enhancing discontinuities via the differential advection process. Transilient turbulence arrays could be made to simulate such structures if the appropriate mixing physics could be translated into a transilient framework. The present papers will be restricted to turbulence processes that increase randomness.

6. Application of turbulent adjustment to nocturnal boundary layers

The responsive transilient mixing process shown in the companion paper becomes increasingly time consuming as the number of grid points increases and the timestep becomes smaller. For higher-resolution models it is often advantageous to switch to a one- or two-pass TA scheme. Although such a TA usually cannot eliminate dynamic instabilities simultaneously over the whole column like transilient mixing can, its slower tendency towards dynamic stability can be offset by the shorter timestep and more frequent application of TA in those models.

A two-pass TA is demonstrated here using a 50 grid-point one-dimensional boundary layer model. Daytime mixed layers are explicitly parameterized using a slab model. Nighttime turbulence, as well as daytime turbulence above the mixed layer, are parameterized using TA. There is no K-theory or other explicit diffusion or smoothing mechanisms in this approach. At night, surface fluxes are injected into the lowest grid layer only; TA is required for any further mixing away from the ground. Model details are described in Appendix B.

Turbulent adjustment is applied after each one-minute timestep. During the first pass, those pairs of grid points with $R_B < R_c$ are adjusted to a state where $R_B = R_T$. During the second pass, all points with $R_B < R_T$ are adjusted to a state where $R_B = R_T$ if those points were either adjusted during the first pass, or were adjacent to adjusted points.

A physical interpretation of this scheme is that any flow with R_B below some termination value R_T can potentially support turbulence if a trigger mechanism

TABLE 1. Model parameters and boundary conditions used for the Wangara day 33–34 case study of turbulent adjustment: w_s is 500 mb subsidence; U_G and V_G are geostrophic winds. Cumulus cloud covers, σ_T and σ_A, are zero. Layer clouds, σ_M and σ_H, are zero except between 1600–1900 when $\sigma_H = 0.05$.

Local time	w_s (mb s^{-1})	U_G, V_G (m s^{-1}) at surface	U_G, V_G (m s^{-1}) at 2 km
	Boundary conditions		
0600	0.0002	−3.76, 1.13	0.6, 0.2
0900	0.0002	−5.34, −0.43	−0.87, −0.21
1200	0.0002	−5.56, 1.27	−1.1, −0.7
1500	0.0002	−6.20, 0.98	−1.4, −1.2
1800	0.0002	−6.42, −0.72	−1.6, −1.7
2100	0.0003	−5.99, −1.93	−1.85, −2.15
0000	0.0003	−6.93, −2.86	−2.5, −2.4
0300	0.0005	−8.02, −3.43	−3.25, −2.7
0600	0.0008	−7.32, −4.97	−3.9, −3.0

Parameters used to determine surface heat fluxes

Name	Value
Latitude/Longitude	34.3°S/144.56°E
Albedo	0.30
Surface relative humidity	25% (used to partition sensible and latent heat)

occurs that can instigate the turbulent breakdown. One trigger mechanism is the Kelvin-Helmholtz wave instabilities that occur whenever R_B is less than a critical value R_c. Another trigger is turbulence itself, if this turbulence is in or adjacent to the potentially unstable flow.

The TA is implemented to first examine all adjacent pairs of grid points to determine which pairs will be adjusted. Then the first pass of the TA adjusts each appropriate pair, starting from the bottom. As discussed earlier, the adjustment of one pair of points often unadjusts the pair just below. After the second pass the grid pairs are closer to being dynamically stable.

Wangara days 33–34 are again used as a case study (Clark *et al.*, 1971). Table 1 shows the parameters and boundary conditions used. The 0600 local time sounding provides the initial conditions for the 24-hour forecast. The results of the potential temperature and wind forecasts are shown in Fig. 2 for $R_c = 1.0$ and $R_T = 2.0$. Sensitivity of TA mixing to choice of critical Richardson number is shown in Fig. 3.

Above the daytime mixed layer there are relatively weak wind shears, so little TA occurs there. However, at night stronger shears associated with nocturnal jet development trigger frequent TA. The resulting temperature profiles show a shallow nocturnal stable layer that strengthens during the night (Stull, 1983). Winds accelerate from their afternoon subgeostrophic values as an inertial oscillation sets up. When the wind shear reaches a sufficient magnitude, TA occurs sporadically and mixes near-surface air higher into the boundary layer.

The purpose of this demonstration is to focus attention on TA and its effects. Surface fluxes and drag are applied to only the lowest grid point. Thus, any variations of the higher grid points in response to nighttime surface fluxes and drag must be directly

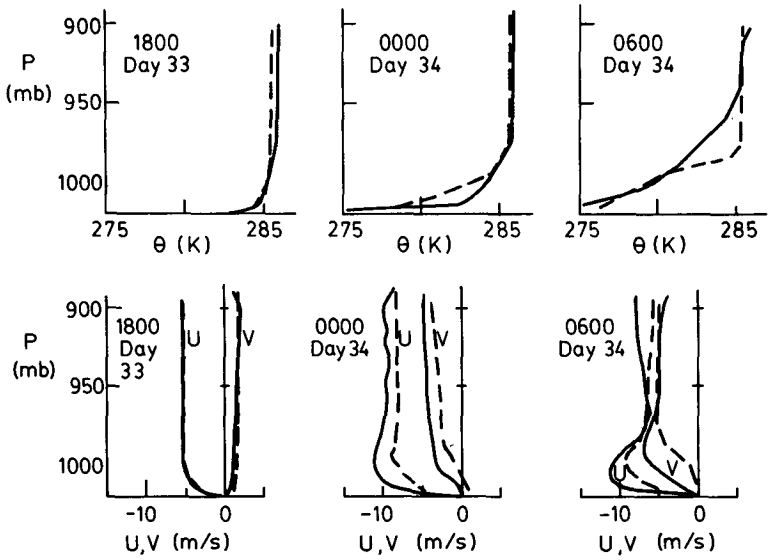

FIG. 2. Forecast of mean potential temperature and winds using a two-pass turbulent adjustment on a 100 m mesh. Solid lines represent observed data, while dashed lines represent model forecasts valid at the corresponding local times. Forecasts were initialized from 0600 Day 33 Wangara data. $R_c = 1.0$; $R_T = 2.0$ (see Fig. 3).

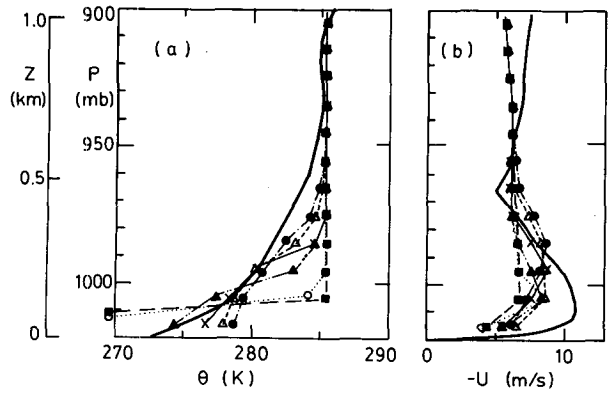

FIG. 3. Sensitivity study of the 24-hour forecast to onset (R_c) and termination (R_T) values of the critical bulk Richardson number for two-pass turbulent adjustment. Using R_c/R_T notation: (open circles) 0.25/1.0; (crosses) 1.0/2.0; (triangles) 1.5/2.0; (solid circles) 2.0/2.0. Two additional forecasts are made using different Richardson numbers for the lowest pair of grid points (R_{cs}, R_{Ts}) than for all other pairs: (solid triangles) R_c/R_T = 1.5/2.0, R_{cs}/R_{Ts} = 0.5/2.0; (solid squares) R_c/R_T = 1.5/3.0, R_{cs}/R_{Ts} = 0.5/3.0. The forecasts are valid for 0600 Day 34 at the Wangara site.

associated with TA. We see from Fig. 2 that wind speeds at the lower grid points are slowed by the effects of surface drag. Also, an apparent interaction between surface influences and the inertial oscillation in the model lead to nocturnal jet formation. Without TA transmitting this surface information up into higher grid points, no jet would form in the model. Instead, the lower grid points would undergo a similar inertial oscillation as the higher grid points, resulting in a more uniform wind profile without a low-level jet.

The importance of turbulence mixing is vividly portrayed in Fig. 3. Small values of R_c lead to less turbulence, making a very shallow layer respond to surface forcings. Larger R_c allow more turbulence, causing the jet max to be less intense and to be higher above ground. Surprisingly, an increase of turbulent mixing above the surface causes less turbulent mixing at the surface, resulting in a very shallow response to surface forcings.

7. Turbulent adjustment efficiency

For mixing between only two grid points, TA is identical to transilient mixing. Mixing among more than two adjacent points is only approximated by TA, meaning that TA is inefficient for modeling large-eddy mixing effects.

In particular, one application of transilient mixing can effect immediate changes at grid point separations equal to the largest eddies modeled. Turbulent adjustment, on the other hand, can transmit information only at the rate of $e\Delta z$ per pass, where Δz is the smallest grid spacing and e represents a TA efficiency (0.0–1.0). Efficiencies less than one are suggested by the "unadjusting" that happens during each TA pass, as discussed earlier. If one defines U_0 as a representative scaling velocity for large-eddy turbulence, then the number N of TA passes needed to achieve mixing equivalent to transilient mixing is on the order of $N = U_0\Delta t/(e\Delta z)$ where Δt is the timestep interval.

A two-pass TA is used in this demonstration model. One-pass TA per timestep was tested (although not shown in this paper) and found to be inadequate. Using N = 2, Δt = 60 s, U_0 = 1 m s^{-1} and Δz = 100 m yields an efficiency estimate of e = 30%. This is obviously just a very rough estimate, but it is useful when designing numerical models that use TA.

One must weigh this TA inefficiency against the typical timescales for changes in mean variables forced by external influences. For example, the above equation can be rewritten in the form of a response time τ_R for TA to eliminate dynamic instabilities: $\tau_R = U_0(\Delta t)^2(eN\Delta z)$. Thus, a model with Δz = 10 m, Δt = 60 s, N = 1, U_0 = 1 m s^{-1} and e = 30% would have a response time of 20 min. If the timescale of change of external forcings is greater than 20 min, then the TA should be able to "catch-up" with these forcings and maintain the proper amount of turbulent mixing to keep the mean flow in dynamic equilibrium.

In spite of TA inefficiency, it is trivial to code and relatively fast to execute on computers for modeling the effects of turbulence. It is particularly useful in numerical models with large numbers of grid points in the vertical and with small timesteps.

8. Discussion and conclusions

Turbulent adjustment is a first-order scheme for parameterizing the sporadic influences of turbulence on the mean flow. Dynamic flow instabilities, as indicated by the Richardson number, are reduced by a TA mixing process between adjacent grid points. This adjustment tends to bring the flow back towards a dynamically stable state if one assumes that winds are mixed to the same proportion as temperatures. Namely, mixing reduces shears and lapse rates proportionally, but the Richardson number becomes larger by this mixing because wind shear is squared in the denominator, but lapse rate is only to the first power in the numerator.

Responsive transilient mixing is more appropriate for coarse-mesh numerical models taking large timesteps. The large-eddy effects that are easily modelled with transilient mixing allow easy simulation of both daytime mixed layers and nocturnal stable layers, without specifically parameterizing those phenomena.

Both TA and this type of responsive transilient mixing apply to only vertical mixing. This is because they are based on the Richardson number. Although turbulence may be set off by dynamic instabilities in the vertical, the resulting turbulence tends to become isotropic for the smaller imbedded eddies. Thus, it is possible to forsee a three-dimensional numerical model that parameterizes horizontal mixing at those grid points undergoing vertical mixing.

Both TA and responsive transilient mixing are generic schemes for which the dynamic-instability-based vertical mixing is just one example. Another brand of responsive transilient mixing might be based on baroclinic instabilities that cause large-eddy mixing such as synoptic-scale cyclones and anticyclones. This scheme could be used as an alternative to geostrophic turbulence schemes (e.g., Hoyer and Sadourny, 1982) to parameterize synoptic-scale horizontal transport in global climate models. Other responsive forms could be based on instabilities in the fluid flow, as indicated by the Reynolds number or Rayleigh number.

Multiple-pass TA has a major drawback compared to transilient mixing in that the large-eddy mixing is only approximated. Namely, TA mixing from grid point 2 to grid point 8 is accomplished only by first mixing into the intermediate points. Transilient mixing, however, can model direct mixing between points 2 and 8, as exemplified by some of the convective overturning examples.

Neither method needs a separate forecast equation for the boundary layer depth. The TA approach, however, may give a depth that lags behind the true depth if timestep and grid-spacing increments are not properly chosen to counteract the inefficiency of TA. In other words, TA might communicate surface forcings to the rest of the mixed layer so slowly that the bottom of the mixed layer would be much too warm while the top would be too cool.

The TA and transilient theory forecasts of Wangara day 33 are of comparable quality with other models (Manins, 1982; Deardorff, 1974; André *et al.*, 1978). Temperatures, wind and mixed-layer depths are generally accurate during the day, within about 0.5 K, 1 m s^{-1}, and 100 m. Nighttime simulations are less accurate, as also displayed by the other models: 1–2 K, 2–3 m s^{-1}, 100 m.

Transilient turbulence theory and turbulent adjustment are obviously not cure-alls for all turbulence situations; they are just tools. The demonstrations in this paper are meant to portray some of the utility of these tools.

Acknowledgments. Eva Singer typed this manuscript with her usual efficiency and speed. NSF supported this research under grants ATM-8012699 and ATM-8210685. The Osaka Gas Company supported the second author's dispersion studies in the United States.

APPENDIX A

Sample Sounding Data

For some soundings, turbulent adjustment might never eliminate dynamic instabilities in one pass. In other words, it might be impossible to find transilient coefficients of a tridiagonal matrix such that all dynamic instabilities are eliminated. An example of such a sounding and the corresponding initial Richardson number profile is given below for a grid spacing of $\Delta z = 10$ m. Let $R_c = 1.0$ and $R_T = 2.5$ in this example.

θ (K)	U (m s^{-1})	R_B
301	15	
		0.33
300	14	
		0.04
298	10	
		0.33
294	8	
		0.67
292	7	

Uniform mixing of adjacent grid points does not work. For example, application of a transilient matrix with all tridiagonal elements equal to ⅓ (except the corner elements, which equal ⅔) gives

θ' (K)	U' (m s^{-1})	R'_B
300.67	14.67	
		0.12
299.67	13.00	
		0.14
297.33	10.67	
		0.16
294.67	8.33	
		0.67
292.67	7.33	

which continues to be unstable.

Even an extreme case of

$$\mathbf{C}(1) = \begin{bmatrix} 0.5 & 0.5 & 0 & 0 & 0 \\ 0.5 & 0 & 0.5 & 0 & 0 \\ 0 & 0.5 & 0 & 0.5 & 0 \\ 0 & 0 & 0.5 & 0 & 0.5 \\ 0 & 0 & 0 & 0.5 & 0.5 \end{bmatrix}$$

yields

θ' (K)	U' (m s^{-1})	R'_B
300.5	14.5	
		0.08
299.5	12.5	
		0.37
297.0	11.0	
		0.11
295.0	8.5	
		0.67
293.0	7.5	

which also fails to be dynamically stable.

Thus, one sees that mixing between more than just neighboring grid points is needed to eliminate dynamic instabilities in some cases. This implies that a single-pass turbulent adjustment would not eliminate dynamic instabilities.

As an example of the effects of large-eddy mixing, application of the following transilient array

$$\mathbf{C}(1) = \begin{bmatrix} 0.22 & 0.21 & 0.20 & 0.19 & 0.18 \\ 0.21 & 0.21 & 0.20 & 0.19 & 0.19 \\ 0.20 & 0.20 & 0.20 & 0.20 & 0.20 \\ 0.19 & 0.19 & 0.20 & 0.21 & 0.21 \\ 0.18 & 0.19 & 0.20 & 0.21 & 0.22 \end{bmatrix}$$

yields

θ (K)	U (m s^{-1})	R'_B
297.24	11.02	
		4.64
297.15	10.94	
		2.53
297.00	10.80	
		2.53
296.85	10.66	
		4.64
296.76	10.58	

which is dynamically stable. In a turbulent adjustment scheme, this large-eddy mixing could be accomplished using multiple passes.

APPENDIX B

Boundary Layer Model Structure and Parameterizations

This model is a one-dimensional, primitive-equation, finite-difference model of the lowest 500 mb of the atmosphere. The height coordinate $\tilde{z}_n$ is defined as the pressure difference between the surface pressure p^B and the pressure at the nth grid point p_n. Thus, $\tilde{z}_n$ is zero at the earth's surface and is positive above ground. The geometric height z is found hydrostatically from $\tilde{z}$. It is impossible to forecast the surface pressure using the model because of its limited vertical domain and one-dimensionality. In the model p^B is held constant at the value reported in the surface weather observation that was used to initialize the model. All heights and velocities are based on geometric length units unless they appear with a ($\tilde{}$), which means pressure units. The superscripts B and T denote values at the bottom and top of the mixed layer.

There are 50 layers in the model, each defined to be 10 mb thick ($\Delta\tilde{z} \equiv 10$ mb). A staggered grid arrangement is used. The horizontal wind components (U, V), potential temperature (θ), pollutant concentration (c), and specific humidity (q) are evaluated at the mass center of each layer. Geopotential height (z) and vertical velocity ($\tilde{w}$) are evaluated at a level representing the top of each layer. Note that $\tilde{w}$ has units of mb s^{-1} and is positive for upward moving air. Grid point indexing starts at the bottom, with the lowest layer and its associated top level indexed as 1. The bottom level of this lowest layer, which represents the earth's surface, has a grid index of 0. A bottom boundary condition of $\tilde{z} = \tilde{w} = 0$ is used at $n = 0$, hence no allowance is made for terrain slope. The variables associated with these 50 grid points will be called the field variables. Grid spacing as well as the total number of grid points is easily changed.

Mixed layer (ML) information is stored as separate variables at one independent grid point. The U, V, θ, q and c values within the ML are assumed to be constant with height, for simplicity. The average height of the mixed layer $\tilde{z}_i$ as well as the index of the field grid layer occupied by the ML top n_{ML} are also stored.

The ML values that are forecast for this one grid point are then copied into all of the field grid points that are below the ML top. Such a copying procedure is efficient, and it saves computer time by eliminating prognostic equations to be solved for each of the affected grid points. This is different than Deardorff's (1972) proposal, where ML and field forecasts were found independently for the same domain and then periodically reconciled. As the ML grows within the present model, more field grid points become imbedded within the ML. As the ML shrinks, such as occurs in the evening, those field grid points that are left above the ML top are again subjected to their own prognostic equations, starting from the initial conditions left by the mixed layer.

Except for the evening transition, the ML depth is allowed to increase or decrease smoothly with time. It need not jump from one field grid to the next. This can be pictured as a pointer that moves up or down with time, always pointing to the top of the turbulent layer. Special values of the variables called capping values are also diagnosed, representing the region between the ML top and the next higher standard field grid layer. These capping values smooth the variations that would otherwise occur as the ML pointer rises past any grid point. Values of the vertical gradient of each variable are also diagnosed to facilitate some of the entrainment calculations.

Values of the variables at the field grid points are usually initialized from rawinsonde observations. The modeled domain is assumed to be located at the latitude and longitude appropriate for the rawinsonde observation station. After gross error checking of the data, the pressure, wind direction and speed, dew point and temperature are converted to $\tilde{z}$, U, V, q and θ. Then these new variables are interpolated to the field grid points, and the height of each level is found hydrostatically.

Next, the model is programmed to search through the initial sounding to find the height of the ML. It selects three heights using three different criteria and then discards the resulting highest and lowest heights. The three criteria are the heights where: 1) the potential temperature first becomes warmer than the shelter-height (surface) potential temperature; 2) the lapse rate first becomes statically stable and 3) the potential temperature becomes 0.5 K warmer than the lowest potential temperature at all lower heights. The initial ML height is thus forced to start at a grid point location.

Centered time differencing is used with the vertical advection and Coriolis terms, while forward time differencing is applied with the diffusion and cloud-forcing terms. Simple numerical stability calculations suggest that the following are required for stable solutions: $|\tilde{w}| < 0.08$ mb s^{-1} for vertical advection

and $\Delta t < 10^4$ s for Coriolis terms, where Δt is the timestep increment. The typical or maximum (as appropriate) values expected to occur in the model are $\tilde{w}_{max} \approx 0.05$ mb s^{-1}, $\Delta t = 60$ s. The model is numerically stable, as verified by many runs.

The continuity equation for the ML is used to forecast the ML thickness (z_i):

$$Dz_i/Dt = w_e(1 - \sigma_A) - w_c{}^T\sigma_A + w_s{}^T,$$

where w_e is the entrainment velocity, σ_A is the cloud cover of active fair-weather cumulus clouds, and D/Dt represents a total derivative applied to horizontal motions only. To properly account for all the mass in the ML, z_i is extended to cover the total horizontal domain, not just the domain between clouds. Entrainment into the ML is assumed to act only between active clouds. A vertical mass flux out of the top of the ML caused by active cloud updrafts is represented by the density times the horizontally-averaged updraft velocity at cloud base $w_c{}^T$. Synoptic-scale vertical velocity imposed at the ML top is $w_s{}^T$, negative for subsidence. Although subsidence is important in controlling the ML depth, magnitudes of subsidence from larger-scale numerical models are of limited accuracy. Subsidence is assumed to be impressed upon the whole ML, regardless of the presence of clouds.

Stull's (1976) entrainment parameterization is used for w_e. Neglecting the gravity-wave term, and combining his energetics form for entrainment with his equation for zero-crossing height of the buoyancy flux, one finds that

$$w_e = \{B + J + [(B + J)^2 + 4BJ/A_1]^{1/2}\}/(2g\Delta\theta_v),$$

where B and J represent buoyant and mechanical contributions to the production of ML turbulence. These contributions can be written as $B = gA_1F_{\theta_v}{}^B$ and $J = (\theta_{vML}/z_i)[A_2C_DM^3 + A_3(\Delta M)^3]$ where A_1, A_2 and A_3 are the empirical coefficients suggested by Stull (1976a). Surface heat fluxes (F), winds (M), and other parameters are described later in this appendix. Entrainment through stratocumulus clouds into the ML is not included in this parameterization for w_e. In cases of weak inversion strengths capping the ML, Deardorff's (1974) recommendation for a constraint on entrainment velocity is slightly modified to be $w_e = 0.2(w_* + u_*)$, where w_* is the free-convection scaling velocity and u_* is the friction velocity.

The surface sensible and latent heat fluxes into the atmosphere at any point over land on the globe are estimated from the solar angle and cloud cover in a manner similar to that of the British operational forecast model (Burridge and Gadd, 1977). Momentum fluxes at the surface are estimated from bulk aerodynamic drag methods. Soil moisture, snow cover and recent rainfall are not accounted for.

The net incoming radiation R in kinematic units (K m s^{-1}) at the earth's surface is

$$R = (1 - \alpha)SE\sin\psi - R_{LW},$$

where α is the albedo, S the solar constant in kinematic units (1.127 K m s^{-1}), E the sky transmission function (dimensionless), ψ the solar angle above the local horizon (set to zero if the sun is below the horizon), and R_{LW} is the effective longwave radiation loss in kinematic units (K m s^{-1}). These, in turn, are parameterized by

$$\left.\begin{aligned} E &= (0.6 + 0.2\sin\psi)(1 - 0.4\sigma_H) \\ &\quad \times (1 - 0.7\sigma_M)(1 - 0.4\sigma_T) \\ R_{LW} &= (0.08\ ^\circ\text{K m s}^{-1}) \\ &\quad \times (1 - 0.1\sigma_H - 0.3\sigma_M - 0.6\sigma_T) \\ \sin\psi &= \sin\delta\sin\phi - \cos\delta\cos\phi\cos(\lambda + \pi H/12) \\ \delta &= \phi_r\cos[2\pi(d - d_r)/d_Y] \end{aligned}\right\},$$

where d is the current day of the year, d_r the day of the summer solstice (197), d_Y the number of days per year (365.25), ϕ_r the latitude of the Tropic of Cancer (23.5°N = 0.4102 rad), δ the solar declination, λ the local longitude (positive east), H time in hours (GMT) and ϕ is the local latitude. The σ_M and σ_H are the middle and high stratiform cloudcover which are supplied as boundary conditions from current and forecast data from other operational models. The total cumuliform cloudcover is σ_T. The parameterizations above imply that surface temperature variations have less effect than cloudcover on longwave radiation lost. A better parameterization would include the surface temperature.

Following Burridge and Gadd (1977), the portion X of the net radiation lost into the ground is assumed to be

$$X = \begin{cases} 0.1 \text{ during daytime} \\ 0.5 \text{ during nighttime.} \end{cases}$$

Thus, the remaining heat flux R' that is available to modify the air is

$$R' = R(1 - X).$$

Deardorff (1978) found this approach to yield acceptable results for models with timestep increments less than about ten minutes. Then R' is partitioned into sensible $F_\theta{}^B$ and latent heat fluxes $LF_q{}^B$, following the suggestion of Wilson and Rouse (1972)

$$\left.\begin{aligned} F_\theta{}^B &= R'/(1 + \beta_s RH^B) \\ F_q{}^B &= (C_p/L)(R' - F_\theta{}^B) \\ \beta &= \epsilon L^2 q_s/(C_p T_{ML}{}^2) \end{aligned}\right\},$$

where RH^B is a representative surface moisture parameter, L the latent heat of vaporization of water, C_p the specific heat of air at constant pressure, ϵ (=0.622) is the gas constant, q_s the saturated specific humidity in the mixed layer, T_{ML} the absolute

temperature of the mixed layer and β_s is $(L/C_p) \times (\partial q_s/\partial T)_p$.

The free convection scaling velocity w_* is found from

$$w_*^3 = (gz_i/\theta_{vML})F_{\theta_v}{}^B,$$

where the mixed-layer virtual potential temperature θ_{vML} is

$$\theta_{vML} = \theta_{ML}(1 + 0.61q_{ML}).$$

The surface virtual potential-temperature flux is

$$F_{\theta_v}{}^B = F_\theta{}^B(1 + 0.61q_{ML}) + 0.61\theta_{ML}F_q{}^B,$$

where q_{ML} and θ_{ML} are the mixed-layer specific humidity and potential temperature.

The friction velocity, u_*, is written as

$$u_*^2 = C_D M^2,$$

where the mixed-layer wind magnitude M is

$$M^2 = U_{ML}^2 + V_{ML}^2$$

for mixed layer wind components U_{ML} and V_{ML}, while the surface kinematic momentum fluxes are

$$\left.\begin{aligned} F_u{}^B &= -C_D U_{ML} M \\ F_v{}^B &= -C_D V_{ML} M \end{aligned}\right\}.$$

A drag coefficient C_D ($=2 \times 10^{-3}$) is used, based on the flat terrain estimates compiled by Garratt (1977). His estimates have been adjusted to account for the fact that ML winds, rather than 10 m-height winds, are used to find the stress. Prognostic equations for the daytime ML variables are

$$\left.\begin{aligned} D\theta_{ML}/Dt &= (F_\theta{}^B - F_\theta{}^T)/z_i \\ Dq_{ML}/Dt &= (F_q{}^B - F_q{}^T)/z_i \\ Dc_{ML}/Dt &= (F_c{}^B - F_c{}^T)/z_i \\ DU_{ML}/Dt &= (F_u{}^B - F_u{}^T)/z_i - f(V_{GML} - V_{ML}) \\ DV_{ML}/Dt &= (F_v{}^B - F_v{}^T)/z_i + f(U_{GML} - U_{ML}) \end{aligned}\right\},$$

where $D/Dt = \partial/\partial t + u\partial/\partial t + v\partial/\partial y$ denotes a total derivative applied only to horizontal motions. The ML-averaged geostrophic wind components (U_{GML}, V_{GML}) must be supplied as time-varying boundary conditions.

During the daytime, fluxes at the top of the mixed layer F^T are assumed to be caused by entrainment of air into the mixed layer between clouds:

$$F_\xi{}^T = -w_e\Delta\xi(1 - \sigma_A),$$

where ξ represents any variable such as potential temperature and $\Delta\xi$ is the value of ξ just above (capping) the ML minus the ML value. Although there are also fluxes caused by the clouds drawing air out of the top of the ML, these fluxes do not directly change the values of the primary ML variables.

At nighttime, the ML is forced to be one grid-layer thick. The model is thus not shocked by any sudden changes in equation format used for the ML. The ML exists both day and night in the model equations, although at night the overall model behavior is identical to that with no ML. This desirable feature allows a straightforward structure to the computer code. It also allows forcings to be made to the bottom of the nocturnal BL via the existing ML bottom boundary parameterizations.

When morning arrives, the sign of the surface heat flux switches from negative to positive. The exact time of this switch depends on many factors, including latitude and cloud cover. This switch signals the model to allow the ML to grow from its previously captive thickness of one grid layer. The equations for the grid points above this ML remain unchanged until the ML top rises past them. At the time each grid point is overtaken by the ML, solution of the prognostic equations for that grid point is suspended. For those grid points, a copying procedure is used, as is described in the daytime subsection.

Above the ML for both day and night situations, the forecast equations are

$$\left.\begin{aligned} d\theta/dt &= 0 \\ dq/dt &= 0 \\ dc/dt &= 0 \\ dU/dt &= -f(V_G - V) \\ dV/dt &= +f(U_G - U) \end{aligned}\right\}.$$

There is no K-theory diffusion in the model (Deardorff and Mahrt, 1982). Instead, mixing is accomplished with the turbulent adjustment procedure discussed at length in the body of this paper.

REFERENCES

André, J. C., G. DeMoor, P. Lacarrère, G. Therry and R. du Vochat, 1978: Modeling the 24-hour evolution of the mean and turbulent structure of the planetary boundary layer. *J. Atmos. Sci.*, **35**, 1861–1883.

Burridge, D. M., and A. J. Gadd, 1977: *The Meteorological Office Operational 10-Level Numerical Weather Prediction Model (December 1975).* Meteorological Office Sci. Pap. No. 34. HMSO, London, 57 pp.

Cahir, J. J., J. M. Norman, W. D. Lottes and J. A. Toth, 1976: New tools for forecasters: real time cross-sections produced in the field. *Bull. Amer. Meteor. Soc.*, **57**, 1426–1433.

Clarke, R. H., A. J. Dyer, R. R. Brook, D. G. Reid, and A. J. Troup, 1971: *The Wangara Experiment: Boundary Layer Data.* Div. Meteor. Phys. Tech. Pap. No. 19, CSIRO, Australia, 316 pp. [NTIS N71-37838.]

Deardorff, J. W., 1972: Parameterization of the planetary boundary layer for use in general circulation models. *Mon. Wea. Rev.*, **100**, 93–106.

——, 1974: Three-dimensional numerical study of the height and mean structure of a heated planetary boundary layer. *Boundary-Layer Meteor.*, **7**, 81–106.

——, 1978: Efficient prediction of ground surface temperature and moisture, with inclusion of a layer of vegetation. *J. Geophys. Res.*, **83**, 1889–1903.

——, and L. Mahrt, 1982: On the dichotomy in theoretical treatments of the atmospheric boundary layer. *J. Atmos. Sci.*, **39,** 2096–2098.

Fiedler, B. H., 1984: An integral closure model for the vertical turbulent flux of a scalar in a mixed layer. *J. Atmos. Sci.*, **41,** 674–680.

Garratt, J. R., 1977: Review of drag coefficients over oceans and continents. *Mon. Wea. Rev.*, **105,** 915–929.

Hoyer, J.-M., and R. Sadourny, 1982: Closure modeling of fully developed baroclinic instability. *J. Atmos. Sci.*, **39,** 707–721.

Kaimal, J. C., and J. A. Businger, 1970: Case studies of a convective plume and a dust devil. *J. Appl. Meteor.*, **9,** 612–620.

Klemp, J. B., and D. K. Lilly, 1978: Numerical simulation of hydrostatic mountain waves. *J. Atmos. Sci.*, **35,** 78–107.

Lenschow, D. H., 1970: Airplane measurements of planetary boundary layer structure. *J. Appl. Meteor.*, **9,** 874–884.

Mahrt, L., 1981: Modelling the depth of the stable boundary layer. *Boundary-Layer Meteor.*, **21,** 3–19.

Manabe, S., S. Smagorinsky and R. F. Strickler, 1965: Simulated climatology of a general circulation model with a hydrologic cycle. *Mon. Wea. Rev.*, **93,** 769–798.

Manins, P. C., 1982: The daytime planetary boundary layer: A new interpretation of Wangara data. *Quart. J. Roy. Meteor. Soc.*, **108,** 689–705.

Stull, R. B., 1976: The energetics of entrainment across a density interface. *J. Atmos. Sci.*, **33,** 1260–1267.

——, 1983: Integral scales for the nocturnal boundary layer. Part I: Empirical depth relationships. *J. Clim. Appl. Meteor.*, **22,** 673–686.

Thompson, R. O. R. Y., 1973: Stratified Ekman boundary layer models. *Geophys. Fluid Dyn.*, **5,** 201–210.

Wilson, R. G., and W. R. Rouse, 1972: Moisture and temperature limits of the equilibrium evapotranspiration model. *J. Appl. Meteor.*, **11,** 436–442.

Woods, J. D., 1969: On Richardson's number as a criterion for laminar-turbulent-laminar transition in the ocean and atmosphere. *Radio Sci.*, **4,** 1289–1298.